

UKAEA-CCFE-PR(19)40

Pui-Wai Ma, S. L. Dudarev

**CALANIE: anisotropic elastic
correction to the total energy, to
mitigate the effect of periodic
boundary conditions**

Enquiries about copyright and reproduction should in the first instance be addressed to the
UKAEA
Publications Officer, Culham Science Centre, Building K1/0/83 Abingdon, Oxfordshire,
OX14 3DB, UK. The United Kingdom Atomic Energy Authority is the copyright holder.

CALANIE: anisotropic elastic correction to the total energy, to mitigate the effect of periodic boundary conditions

Pui-Wai Ma, S. L. Dudarev

CALANIE: anisotropic elastic correction to the total energy, to mitigate the effect of periodic boundary conditions

Pui-Wai Ma

Culham Centre for Fusion Energy, UK Atomic Energy Authority, Culham Science Centre, Abingdon, Oxfordshire, OX14 3DB, United Kingdom

S. L. Dudarev

Culham Centre for Fusion Energy, UK Atomic Energy Authority, Culham Science Centre, Abingdon, Oxfordshire, OX14 3DB, United Kingdom

Abstract

CALANIE (CALculation of ANIsotropic Elastic energy) program evaluates an elastic interaction correction to the total energy of a localized object, for example a defect in a solid material simulated using an *ab initio* or molecular statics approach, resulting from the use of periodic boundary conditions. The correction, computed using a fully elastically anisotropic Green's function formalism, arises from the elastic interaction between a defect and its own periodically translated images. The field of elastic displacements produced by the defect is described in the elastic dipole approximation. Applications of the method are illustrated by two case studies, one involving an *ab initio* investigation of point defects and vacancy migration in FCC gold, and another a molecular statics simulation of a dislocation loop. We investigate the convergence of the method as a function of the simulation cell size, and note the particular significance of elastic correction in the limit where the size of the defect is comparable with the size of the simulation cell.

Keywords: Point defects, elastic dipole tensor, anisotropic elasticity, periodic boundary conditions, *ab initio* calculations

Email addresses: `leo.ma@ukaea.uk` (Pui-Wai Ma), `sergei.dudarev@ukaea.uk` (S. L. Dudarev)

PROGRAM SUMMARY

Manuscript Title: CALANIE: anisotropic elastic correction to the total energy, to mitigate the effect of periodic boundary conditions

Authors: Pui-Wai Ma, S. L. Dudarev

Program Title: CALANIE, version 2.0

Journal Reference:

Catalogue identifier:

Licensing provisions: Apache License, Version 2.0

Programming language: C/C++

Computer: Any computer with C/C++ compiler

Operating system: Linux, Unix, Windows

RAM: 15MB

Number of processors used: 1

Supplementary material:

Keywords: Defects, dipole tensor, elastic correction, anisotropy elasticity, *ab initio* calculations, periodic boundary conditions

Classification: 7.1

External routines/libraries:

Subprograms used:

Nature of problem:

Periodic boundary conditions (PBCs) are often used in the context of *ab initio* and interatomic potential based atomic scale simulations. A localized defect in a crystalline material, simulated using PBCs, interacts elastically with its own periodically translated images, and this gives rise to a systematic error in the computed defect formation or migration energy. Evaluating the correction to the total energy resulting from effects of elastic interaction between a defect and its periodic images, to alleviate the effect of PBCs, is an essential aspect of any accurate calculation of the energy of a defect performed using PBCs.

Solution method:

The energy of interaction between a localized defect and its periodically translated images is computed in the linear elasticity approximation. In this approximation, the energy of elastic interaction is expressed analytically in terms of the elastic dipole tensor of the defect and elastic Green's function. Elements of the dipole tensor are computed as a part of the simulation evaluating the formation energy of the defect. Elastic Green's function and its first and second derivatives are computed numerically from the elastic constants of the material. The method and the corresponding numerical procedures are implemented in the CALANIE computer program. The program evaluates matrix elements of the elastic dipole tensor of a localized defect and the elastic correction to the total energy arising from the use

41 of periodic boundary conditions.

42

43 *Restrictions:*

44 The approach assumes the validity of the linear elasticity approximation. This
45 limits the accuracy of evaluation of the elastic correction, which becomes less pre-
46 cise if the size of the defect is comparable with the size of the simulation cell.

47

48 *Unusual features:*

49 An open source code, containing full detail of the relevant theoretical concepts,
50 algorithms and numerical implementation.

51

52 *Running time:* A typical calculation takes several minutes.

53

54

55 **1. Introduction**

56 Mechanical deformation or irradiation by energetic particles produce de-
57 fects in a crystalline material, such as dislocations, dislocation loops, voids,
58 and Frenkel pairs [1, 2, 3, 4]. Defect structures evolve under the effect of ex-
59 ternal stress and temperature. Defects migrate, segregate and agglomerate as
60 a result of elastic interaction, mediated by lattice deformations [5, 6, 7, 8, 9].
61 Evolution of defect structures changes mechanical and physical properties of
62 the material [10].

63 Electronic and atomic scale simulations are indispensable numerical tools
64 that help understand the fundamental laws driving microstructure evolution
65 and its effect on mechanical and physical properties of the materials. *Ab ini-*
66 *tio* density function theory (DFT) calculations [11, 12] are commonly used for
67 computing the formation and migration energies of small defects. The energy
68 of formation of a defect at equilibrium determines the relative probability of
69 its occurrence, whereas the energy of migration determines the rate of evolu-
70 tion of a defect structure. Molecular dynamics [2, 3] and kinetic Monte Carlo
71 [13, 14, 15] simulations provide information about the rates and pathways of
72 relaxation processes characterizing complex configurations of defects.

73 To avoid considering surface effects, simulations are often performed us-
74 ing periodic boundary conditions (PBCs). Through periodic boundary con-
75 ditions, a spatially localized defect situated in a simulation cell interacts
76 elastically with an infinite number of its own images situated in periodically

77 translated simulation cells [6, 7, 8, 9]. Since elastic fields effectively have infi-
78 nite range, and the energy E_{el} of elastic interaction between any two defects
79 varies as the inverse cube of distance R between the defects $E_{el} \sim R^{-3}$ [8],
80 if a relatively small cell is used in a simulation, the elastic energy of interac-
81 tion between a defect and its periodic images can be substantial. This can
82 affect the accuracy of calculations performed using PBCs and make the total
83 energy data strongly dependent on the cell size. Although in principle the
84 issue can be circumvented using a larger simulation cell, in practice this may
85 not necessarily be a realistic option because of the limitations imposed by
86 the available computational resources or numerical algorithms. For example,
87 in a conventional DFT calculation, the simulation cell size is still limited to
88 a few hundred atoms.

89 A possible way forward is to introduce an elastic correction to the calcu-
90 lated formation energy. A first order correction, in the linear elasticity far
91 field approximation, can be derived using the elastic dipole tensor formalism
92 [6, 7, 8, 9], which only requires knowing the elements of elastic dipole tensor
93 P_{ij} of the defect and the elastic constants tensor C_{ijkl} of specific material.
94 This information can be readily derived from the same DFT or molecular
95 statics calculation.

96 An elastic dipole tensor fully defines the elastic field produced by a defect
97 in a material [16]. The strain field associated with a localized defect can
98 be expressed in an explicit analytical manner in terms of the dipole tensor.
99 From the dipole tensor it is also possible to evaluate the relaxation volume
100 tensor of the defect [17]. By considering a defect as a compound object
101 characterized by its dipole tensor, it is possible to formulate a continuum
102 model spanning the spatial scale many orders of magnitude larger than an
103 atomistic simulation. In addition, the notion of the dipole tensor enables
104 treating interactions between defects. A dipole tensor can be defined for
105 an arbitrarily large configuration of defects, for example the entire defect
106 structure created in a collision cascade simulation can be described by a
107 dipole tensor, enabling extending the treatment to a macroscopic scale [17].

108 In previous studies, we derived analytical equations for treating the elas-
109 tic fields of defects in a simulation cell using periodic boundary conditions
110 [8]. We have also derived equations for evaluating the elastic correction to
111 the energy of a localized defect [9], and implemented them in our program
112 CALANIE. It is appropriate to make this code, suitable for evaluating the
113 elastic correction to the total energy, and for calculating the elastic dipole
114 tensor of a defect in a simulation cell, available as an open source computer

115 program. Full numerical and algorithmic aspects of the code are described
 116 below.

117 In what follows we review our theory and explain the meaning of various
 118 equations. We also discuss the details of the numerical implementation of the
 119 method, followed by the details of the compilation procedure, and the format
 120 of input and output files. We give two examples illustrating applications of
 121 the code. The first example involves *ab initio* calculations of properties of
 122 point defects and vacancy migration in FCC gold. This example illustrates
 123 the applicability of CALANIE to both equilibrium and non-equilibrium con-
 124 figurations. The second example illustrates molecular statics calculations
 125 of mecoscopic size dislocation loops. We investigate the convergence of the
 126 dipole tensor and the formation energy of defects as functions of the sim-
 127 ulation box size, and the significance of applying elastic correction to the
 128 formation energy in the limit where the simulation cell is relatively small.

129 2. Theory

130 2.1. Elastic dipole tensor

131 In continuum elasticity theory, the elastic strain energy of a defect in an
 132 infinite medium is defined as a volume integral over the entire space:

$$E_D = \frac{1}{2} \int_V \sigma_{ij}(\mathbf{r}) \epsilon_{ij}(\mathbf{r}) dV, \quad (1)$$

133 where ϵ_{ij} and σ_{ij} are the elastic strain and stress fields. Assuming the validity
 134 of the linear elasticity approximation, we write $\sigma_{ij} = C_{ijkl} \epsilon_{kl}$, where C_{ijkl} is
 135 the elastic constant tensor of rank four. The above equation now acquires
 136 the form

$$E_D = \frac{1}{2} \int_V C_{ijkl} \epsilon_{kl}(\mathbf{r}) \epsilon_{ij}(\mathbf{r}) dV. \quad (2)$$

137 In the presence of infinitesimal external strain ϵ_{ij}^{ext} , elastic energy E_D can be
 138 represented by a Taylor series expansion:

$$E_D(\epsilon_{ij}^{ext}) = E_D(\epsilon_{ij}^{ext} = 0) + \left(\frac{\delta E_D}{\delta \epsilon_{ij}^{ext}} \right)_{\epsilon_{ij}^{ext}=0} \epsilon_{ij}^{ext} + \dots \quad (3)$$

139 The energy of elastic interaction between a defect and external strain field is
 140 defined as [16]:

$$E = -P_{ij} \epsilon_{ij}^{ext}, \quad (4)$$

141 where P_{ij} is the elastic dipole tensor of a defect. Comparing Eq. 3 and 4, we
 142 can identify the dipole tensor with

$$P_{ij} = - \left(\frac{\delta E_D}{\delta \epsilon_{ij}^{ext}} \right)_{\epsilon_{ij}^{ext}=0} = - \int_V \sigma_{ij}^D dV, \quad (5)$$

143 where σ_{ij}^D is the stress field resulting from the presence of a defect in the
 144 elastic medium.

145 In practice, calculations are not performed in an infinite medium. Infinite
 146 medium is simulated by applying periodic boundary conditions to a finite size
 147 simulation cell. This is equivalent to putting N identical defects in an infinite
 148 medium in the form of a lattice of defects, defined by the translation vectors
 149 of the simulation cell, where $N \rightarrow \infty$. We can write the total stress as a linear
 150 sum of contributions from all the identical periodically translated defects as
 151 [8],

$$\int_V \sigma_{ij}^D dV + \sum_{n \neq 0} \int_V \sigma_{ij}^{Im,n} dV = N \int_V \sigma_{ij}^D dV, \quad (6)$$

152 where $\sigma_{ij}^{Im,n}$ is the stress field due to the n^{th} image of the defect. Dividing
 153 both sides of the above equation by N , we find

$$\int_V \sigma_{ij}^D dV = \frac{1}{N} \int_V \left(\sigma_{ij}^D + \sum_{n \neq 0} \sigma_{ij}^{Im,n} \right) dV = \int_{V_{cell}} \sigma_{ij} dV. \quad (7)$$

154 Therefore, the total stress induced by a defect integrated over infinite medium
 155 equals the total stress of the defect plus all its images, integrated over a
 156 simulation cell in a periodic boundary condition calculation. The proof is
 157 based on the linear elasticity approximation stating that the total stress field
 158 is a linear sum of stresses produced by the defect and all its images, and
 159 on the fact that the stress field in a simulation cell is the same as in any
 160 periodically translated cell. The simulation box used for defect calculation
 161 needs to be of exactly the same shape and volume as in the corresponding
 162 perfect lattice case, to mimic the infinite medium condition.

163 Eq. 5 can now be written in term of macrostress $\bar{\sigma}_{ij}$ developing in a
 164 simulation cell under the PBCs, namely

$$P_{ij} = - \int_{V_{cell}} \sigma_{ij} dV = -V_{cell} \bar{\sigma}_{ij}. \quad (8)$$

165 The macrostress $\bar{\sigma}_{ij}$ is the same as the average stress in the cell. We note that
 166 the volume integral may be ill-defined if the equation is applied to a discrete
 167 atomistic configuration. However, the same expression can be derived in the
 168 discrete atomistic approximation.

169 Provided that the total energy of the system depends only on atomic
 170 positions, such that $E_D = E_D(\{\mathbf{R}_n\})$, where $\{\mathbf{R}_n\}$ is a set of coordinates, we
 171 can write

$$P_{ij} = - \left(\frac{\delta E_D}{\delta \epsilon_{ij}^{ext}} \right)_{\epsilon_{ij}^{ext}=0} = - \sum_{n,\alpha} \frac{\delta E_D}{\delta R_{n,\alpha}} \left(\frac{\delta R_{n,\alpha}}{\delta \epsilon_{ij}^{ext}} \right)_{\epsilon_{ij}^{ext}=0}, \quad (9)$$

172 where n is the index of an atom and α refers to a Cartesian coordinate. This
 173 first term in the right hand side is the component of force $F_{n,\alpha}$ acting on
 174 the atoms. The second term can be obtained assuming that all the position
 175 vectors move in response to the applied external strain:

$$\mathbf{R} \rightarrow (\mathbf{I} + \boldsymbol{\epsilon})\mathbf{R}, \quad (10)$$

176 which leads to

$$\left(\frac{\delta R_{n,\alpha}}{\delta \epsilon_{ij}^{ext}} \right)_{\epsilon_{ij}^{ext}=0} = R_{n,j} \delta_{\alpha i}. \quad (11)$$

177 The dipole tensor then becomes

$$P_{ij} = \sum_n F_{n,i} R_{n,j} = -V_{cell} \bar{\sigma}_{ij}. \quad (12)$$

178 This is the same formula for calculating dipole tensor as found using the
 179 Kanzaki force method [16]. Interestingly, according to the Virial Theorem at
 180 0K, the right hand side can also be written in terms of the macrostress. We
 181 note that in a DFT calculation, the macrostress developing in a cell due to
 182 the presence of a defect in it, is calculated as the variation of the total energy
 183 as a function of the strain tensor. In both the continuum and discrete limits,
 184 we arrive at the same equation for the dipole tensor. This equation relates
 185 linear elasticity to both electronic and atomic scale simulations.

186 If the simulation cell used in the context of defect simulations has a
 187 different shape in comparison with the perfect lattice case, the case can be
 188 treated as if the simulation cell is subjected to external strain. The strain
 189 tensor describing the applied external strain $\boldsymbol{\epsilon}^{app}$, given that $\|\boldsymbol{\epsilon}^{app}\| \ll 1$,
 190 relates the perfect and deformed simulation cells as follows

$$\mathbf{V}^{perf}(\mathbf{I} + \boldsymbol{\epsilon}^{app}) = \mathbf{V}^{def}, \quad (13)$$

191 where \mathbf{I} is the identity matrix, $\mathbf{V}^{perf} = \{\mathbf{L}_1^{perf}, \mathbf{L}_2^{perf}, \mathbf{L}_3^{perf}\}$ is the matrix of
 192 translation vectors of the perfect lattice cell and $\mathbf{V}^{def} = \{\mathbf{L}_1^{def}, \mathbf{L}_2^{def}, \mathbf{L}_3^{def}\}$ is
 193 the matrix of translation vectors of the cell containing a defect. Therefore
 194 the strain tensor is simply

$$\boldsymbol{\epsilon}^{app} = (\mathbf{V}^{perf})^{-1} \mathbf{V}^{def} - \mathbf{I}. \quad (14)$$

195 Whenever applied strain exists, the dipole tensor should be corrected as
 196 [6, 7, 9]

$$P_{ij} = V_{cell}(C_{ijkl}\epsilon_{kl}^{app} - \bar{\sigma}_{ij}). \quad (15)$$

197 There are other methods using which one can derive elastic dipole tensors
 198 from atomic scale simulation [16, 6, 18]. Varvenne and Clouet [7] concluded
 199 that only the residual stress method is tractable in the limit of small simula-
 200 tion cell, especially in the relation to *ab initio* calculations. Below we check
 201 the convergence of P_{ij} , and the effect of cell size on the elastic correction
 202 energy.

203 For a linear defect, such as a self-interstitial atom (SIA) crowdion defect,
 204 we can write [8]:

$$P_{ij} = C_{ijkl} \left(\Omega^{(1)} n_k n_l + \frac{\Omega^{(2)}}{3} \delta_{kl} \right) \quad (16)$$

205 where $\mathbf{n} = (\cos \phi \sin \theta, \sin \phi \sin \theta, \cos \theta)$ is a unit vector characterizing the
 206 orientation of the axis of the defect, and $\Omega^{(1)}$ and $\Omega^{(2)}$ represent the relative
 207 contribution of the anisotropic and isotropic components to the relaxation
 208 volume of a defect, where the total relaxation volume of the defect is given
 209 by the sum

$$\Omega_{rel} = \Omega^{(1)} + \Omega^{(2)}. \quad (17)$$

210 Values of $\Omega^{(1)}$ and $\Omega^{(2)}$ can be obtained from *ab initio* calculations. This
 211 formula is used for analyzing the change in elastic correction energy assuming
 212 that a defect is able to rotate freely [8].

213 2.2. Elastic correction energy

214 The formation energy of a defect equals [9]:

$$E_{def}^F = [E_{def}(N_{def}) - E^{app}] - \frac{N_{def}}{N_{perf}} E_{perf}(N_{perf}) - E_{el}^{corr}, \quad (18)$$

215 where E_{def} is the energy of a simulation cell containing a defect, E_{perf} is the
 216 energy of a reference perfect lattice cell, N_{def} is the number of atoms in the

217 cell containing a defect, N_{perf} is the number of atoms in a perfect lattice cell,
 218 E^{app} is the elastic energy due to the applied strain, and E_{el}^{corr} is the elastic
 219 correction energy due to the PBCs. The applied strain energy equals [6]:

$$E^{app} = \frac{V^{perf}}{2} C_{ijkl} \epsilon_{ij}^{app} \epsilon_{kl}^{app} - P_{ij} \epsilon_{ij}^{app}, \quad (19)$$

220 where V^{ref} is the volume of the simulation cell. We neglect the change of
 221 volume due to deformation assuming small applied strain. The first term in
 222 equation (19) accounts for the elastic energy associated with the deformation
 223 of the simulation cell. The second term is the result of interaction between
 224 the defect and applied strain.

225 The elastic correction energy E_{el}^{corr} is a term resulting from the periodic
 226 supercell effect. It contains two parts

$$E_{el}^{corr} = E_{DD} + E_{strain}^{corr}. \quad (20)$$

227 E_{DD} is the energy due to elastic interaction between a defect and its periodic
 228 images, represented by elastic dipole-dipole terms. E_{strain}^{corr} is the self-strain
 229 correction energy. Adopting the far-field elasticity approximation, the reg-
 230 ularized elastic interaction energy E_{DD} can be written in terms of elastic
 231 dipole tensor and anisotropic elastic Green's function [19, 6, 7, 8], where

$$E_{DD} = E_{DD}^{total} + E_{DD}^{corr}. \quad (21)$$

232 The first term

$$E_{DD}^{total} = \frac{1}{2} \sum_{n \neq 0} P_{ij} P_{kl} \frac{\partial}{\partial x_j} \frac{\partial}{\partial x_l} G_{ik}(\mathbf{R}_n) \quad (22)$$

233 is a sum of pairwise elastic interactions between a defect and its periodic
 234 images situated at \mathbf{R}_n . The sum is conditionally convergent. The second
 235 term

$$E_{DD}^{corr} = -\frac{1}{2V_{cell}} \sum_{n \neq 0} \int_{V_{cell}} P_{ij} P_{kl} \frac{\partial}{\partial x_j} \frac{\partial}{\partial x_l} G_{ik}(\mathbf{R}_n - \mathbf{r}) d^3r \quad (23)$$

236 regularizes the strain produced by the periodic images and ensures the ab-
 237 solute convergence of sum (22).

238 The self-strain correction energy is

$$E_{strain}^{corr} = -\frac{1}{2} P_{ij} (-\bar{\epsilon}_{ij}^D) = \frac{1}{2V_{cell}} \int_{V_{cell}} P_{ij} \epsilon_{ij}^D(\mathbf{r}) d^3r. \quad (24)$$

239 As we only need to correct the linear elastic part of the strain field of the
 240 defect, one can apply the far-field approximation again, namely

$$E_{strain}^{corr} = -\frac{1}{2V_{cell}} \int_{V_{cell}} P_{ij} P_{kl} \frac{\partial}{\partial x_j} \frac{\partial}{\partial x_l} G_{ik}(\mathbf{r}) d^3r. \quad (25)$$

241 This term corrects the total energy for the effect of elastic strain produced by
 242 the defect itself. Eq. (25) has the form similar to Eq. (23), and corresponds
 243 to the first term $n = 0$ in the series.

244 In practice, Eq. (23) and (25) can be represented by surface integrals
 245 through the use of the divergence theorem [20], namely

$$\int_{V_{cell}} P_{kl} \frac{\partial}{\partial x_j} \frac{\partial}{\partial x_l} G_{ik}(\mathbf{r}) d^3r = \oint_{S_{cell}} P_{k\alpha} \frac{\partial}{\partial x_j} G_{ik}(\mathbf{r}) n_\alpha dS. \quad (26)$$

246 Here \mathbf{n} is the unit vector of external surface normal, and index α refers a
 247 Cartesian component of this vector. Calculating the first derivative of elastic
 248 Green's function is numerically more expedient than the second derivative,
 249 and the same applies to the calculation of surface integrals versus volume
 250 integrals. Elastic Green's function, and its first and second derivatives can
 251 be calculated numerically following Barnett's approach [21].

252 3. Algorithm

253 It is not feasible to calculate E_{DD}^{total} and E_{DD}^{corr} by adding up an infinite
 254 number of terms in the series. Provided that we take the same number of
 255 terms in both series, the sum of them, E_{DD} , converges at a large cutoff
 256 distance [8]. Calculating E_{DD}^{total} is trivial, since we can evaluate the second
 257 derivative of elastic Green's function numerically. The calculation of E_{DD}^{corr} is
 258 somewhat more involved as it requires calculating integrals over the surface
 259 of the simulation cell, see Eq. 26.

260 A simulation cell involving PBCs usually has six surfaces. Generally, we
 261 need to consider a surface integral over a rhombohedral cell. For an arbitrary
 262 function F , the surface integral of a rhomboid in three dimensional system
 263 of coordinates can be written as

$$\int_S F(\mathbf{r}(u, v)) dS = \int_{-1}^1 \int_{-1}^1 F(\mathbf{r}(u, v)) J(u, v) du dv \quad (27)$$

264 where

$$J(u, v) = \left\| \frac{\partial \mathbf{r}}{\partial u} \times \frac{\partial \mathbf{r}}{\partial v} \right\| \quad (28)$$

265 is the transformation Jacobian. The position vector \mathbf{r} is a function of u and
 266 v in terms of the translation vectors of the simulation cell. For example, the
 267 position vector at the top and bottom surfaces of a box is

$$\mathbf{r} = \frac{u}{2}\mathbf{L}_x + \frac{v}{2}\mathbf{L}_y \pm \frac{1}{2}\mathbf{L}_z, \quad (29)$$

268 where the $+$ and $-$ signs in the last term correspond to the top and bottom
 269 surfaces, respectively. The Jacobian for both the top and bottom surfaces is
 270 now

$$J(u, v) = \frac{1}{4} \|\mathbf{L}_x \times \mathbf{L}_y\|. \quad (30)$$

271 The Jacobian for the other four surfaces can be evaluated in a similar way.

272 Integration from -1 to 1 is performed numerically using the nine point
 273 Gaussian quadrature method. In the two dimensional case, the double inte-
 274 gration is performed in a nested manner, namely

$$\int_{-1}^1 \int_{-1}^1 f(u, v) dudv \approx \sum_i \sum_j w_i w_j f(u_i, v_j) \quad (31)$$

275 where w_i and w_j are the weights with respect to u_i and v_j . This fully defines
 276 the numerical procedure required for evaluating the surface integral in Eq.
 277 (26). A test involving eleven point Gaussian quadrature integration was also
 278 performed, and procudes the same result up to four decimal places [8].

279 We have verified our calculations of E_{DD} using summation over cubic,
 280 spherical and ellipsoidal summation volumes [8], increasing the magnitude of
 281 the cut-off distance, and found that the results were absolutely convergent in
 282 all cases. Considering the balance between efficiency and accuracy, we chose
 283 to use spherical neighbourhoods with the cutoff radius of $10 + \delta$ times trans-
 284 lation vectors, where the magnitude of δ is small. Our results were verified
 285 numerically against numerical results computed using ANETO [6], which is a
 286 FORTRAN program developed independently by Varvenne *et al.* for a simi-
 287 lar purpose. The authors of Ref. [6] attribute their methodology to Cai *et al.*
 288 [22], who developed it for correcting elastic interactions between dislocations
 289 in two dimensions, using an electrostatic analogy. No electrostatic analogy
 290 was involved in the derivation of equations given in the preceding section of
 291 this paper.

292 4. Compilation of the program

293 CANALIE is a code written in C++. It can be compiled using any
294 modern C++ compiler, including Intel and GNU compilers. No linking to
295 external libraries is required. The code can be compiled in two different ways
296 for two different purposes. The first one is for general *ab initio* calculations.
297 Using g++, one can compile CANALIE using the following command line

```
298 $ g++ -DABINITIO -DSTRESSeV -o calanie CALANIE_2.0.cpp
```

299 OR

```
300 $ g++ -DABINITIO -DSTRESSGPa -o calanie CALANIE_2.0.cpp
```

301 Option -DABINITIO defines the word ABINITIO in the code, such that
302 the program is compiled for the purpose of correcting the elastic energy
303 and obtaining the dipole tensor from the output of a general purpose *ab*
304 *initio* program. Option -DSTRESSeV means that stresses in the input file
305 should be given in eV units. In other words, the input stresses are not the
306 macro-stresses, but rather the macro-stresses multiplied by the cell volume.
307 If one uses VASP [23, 24, 25, 26], the values are given in the line “Total”
308 of the “OUTCAR” file. On the other hand, one can use a more general
309 option -DSTRESSGPa. The stresses in the input file should then be given
310 as the residual stresses, and should have the units of GPa. The sign of
311 stresses follows the convention adopted in VASP. Positive stress means that
312 the simulation cell attempts to expand.

313 The second compilation option is needed for analyzing the relative elastic
314 effect assuming that a linear defect can be rotated. It can be compiled using
315 the command

```
316 $ g++ -DORIENTATION -o calanie CALANIE_2.0.cpp
```

317 This command compilation is required for analyzing changes in elastic cor-
318 rection energy of a defect assuming that it can rotate freely, according to
319 Eq. 16. This enables assessing the stability of a defect under the influ-
320 ence of stresses developing in the supercell under PBCs. Application of this
321 compilation option was illustrated in our earlier work [8].

322 **5. Inputs and outputs**

323 CALANIE requires two input files. They are *input_data* and *input_elastic*.
324 These files need to be located in the same directory for executing CALANIE.
325 Both of them are ASCII files.

326 When we use option -DABINITIO, in the *input_data* file we need to spec-
327 ify the translation vectors, the linear scaling factor, and the residual stresses
328 in the perfect cell and in the cell containing a defect. They should be specified
329 using the following format

```
330     box_ref_11 ???  
331     box_ref_12 ???  
332     box_ref_13 ???  
333     box_ref_21 ???  
334     box_ref_22 ???  
335     box_ref_23 ???  
336     box_ref_31 ???  
337     box_ref_32 ???  
338     box_ref_33 ???  
339     a_lattice_ref ???  
340  
341     box_def_11 ???  
342     ⋮  
343     box_def_33 ???  
344     a_lattice_def ???  
345  
346     stress11_ref ???  
347     ⋮  
348     stress33_ref ???  
349  
350     stress11_def ???  
351     ⋮  
352     stress33_def ???  
353
```

354 The numerical value that follows a keyword is the input value, the position of
355 which is indicated by ??? above. Keywords **box_ref_αβ** and **box_def_αβ**
356 are the translation vectors of the perfect reference cell and the cell containing
357 a defect, and $\alpha, \beta = 1, 2, 3$. Keywords **a_lattice_ref** and **a_lattice_def** are

358 linear scaling factors. Keywords **stress $\alpha\beta$ _ref** and **stress $\alpha\beta$ _def** are the
 359 residual stresses in the reference cell and in a cell containing a defect. One
 360 and only one value should be given. All the nine matrix elements for the
 361 translation vectors and residual stresses are required.

362 In the *input_elastic* file, the first two lines are comment lines. The third
 363 to eighth lines contain values of elastic constants in the Voigt notation C_{ij} ,
 364 in GPa units, followed by the compliance constants S_{ij} , also in the Voigt
 365 notation, in GPa^{-1} units. The input should appear as follows

```

366     #comments
367     #comments
368     C11 C12 C13 C14 C15 C16
369     C21 C22 C23 C24 C25 C26
370     C31 C32 C33 C34 C35 C36
371     C41 C42 C43 C44 C45 C46
372     C51 C52 C53 C54 C55 C56
373     C61 C62 C63 C64 C65 C66
374     S11 S12 S13 S14 S15 S16
375     S21 S22 S23 S24 S25 S26
376     S31 S32 S33 S34 S35 S36
377     S41 S42 S43 S44 S45 S46
378     S51 S52 S53 S54 S55 S56
379     S61 S62 S63 S64 S65 S66

```

380 Once both input files *input_data* and *input_elastic* are available, the program
 381 can be run from the same directory by executing the command

```

382     $ ./calanie

```

383 We provide a simple python script *make_input_elastic.py* to help generate
 384 *input_elastic*. One needs to provide a file with the name *input_elastic_Cij* with
 385 only the first eight lines of *input_elastic*. By running *make_input_elastic.py*,
 386 one generates file *input_elastic* with the required values of S_{ij} . Sample files
 387 with names *input_data_2*, *input_elastic* and *input_elastic_Cij* are included in
 388 the distribution of CALANIE.

389 When using option -DORIENTATION, in *input_data* we only need to
 390 specify the translation vectors and linear scaling factor for the reference cell.
 391 We also need the values of $\Omega^{(1)}$ and $\Omega^{(2)}$ through the keywords of **Omega1**
 392 and **Omega2** in \AA^3 units. A sample file named *input_data_1* illustrates this

	No. of atoms	Approx. cell size	k-points
Vac	107	3x3x3	4x4x4
$\langle 100 \rangle$ d	145	3x3x4	4x4x3
Octa	145	3x3x4	4x4x3
$\langle 110 \rangle$ c	193	3x4x4	4x3x3
$\langle 110 \rangle$ d	193	3x4x4	4x3x3

Table 1: The number of atoms, approximate cell size (in the units of cubic unit cell size), and the k-point mesh that were used in the calculations of vacancy, $\langle 100 \rangle$ dumbbell, octahedral site interstitial, $\langle 110 \rangle$ crowdion, and $\langle 110 \rangle$ dumbbell defects in FCC gold.

393 part of input. The *input_elastic* file is the same as in the previous case.
394 However, when we run the program, we need to specify the orientation of a
395 defect in terms of θ and ϕ , namely

396 `./calanie θ ϕ`

397 The dipole tensor of the defect can be calculated using Eq. 16, followed by
398 the calculation of its elastic correction energy.

399 There is no output file format associated with either option. Outputs
400 are printed out directly. Values of P_{ij} , E^{app} , E_{DD}^{total} , E_{DD}^{corr} , E_{DD} , E_{strain}^{corr} ,
401 and E_{el}^{corr} are computed and displayed. The relaxation volume tensor Ω_{ij}
402 and relaxation volume Ω_{rel} are also evaluated and printed out according to
403 equations $\Omega_{ij} = S_{ijkl}P_{kl}$ and $\Omega_{rel} = \text{Tr}(\Omega_{ij})$.

404 6. Applications

405 6.1. *Ab initio* calculations: Point defects in FCC gold

406 Elastic correction can be readily applied in the context of a calcula-
407 tion of formation and migration energies of point defects. We have applied
408 CALANIE to improve the quality of *ab initio* data on defect energies in
409 FCC gold, which were partially described in a study by Hofmann *et al.* [27].
410 The calculations were performed for vacancy and self-interstitial atom (SIA)
411 defects, where the latter included a $\langle 100 \rangle$ dumbbell, an octahedral site inter-
412 stitial, a $\langle 110 \rangle$ crowdion, and a $\langle 110 \rangle$ dumbbell.

413 All the *ab initio* density functional theory (DFT) calculations were per-
414 formed using Vienna Ab initio Simulation Package (VASP) [23, 24, 25, 26].
415 We used the revised-TPSS exchange-correlation functional [28, 29]. The spin-
416 orbit coupling was also included, to account for the band splitting and shape

	E_{def}	E_{perf}	E^{app}	E_{el}^{corr}	E_{def}^F	E_{def}^F (no corr)
Vac	4056.141572	4093.103600	-0.010717	0.00848	0.939	0.937
$\langle 100 \rangle$ d	5499.210885	5457.464770	-0.273714	0.18303	3.938	3.847
Octa	5499.380148	5457.464770	-0.285801	0.19697	4.105	4.016
$\langle 110 \rangle$ c	7318.341711	7276.601601	-0.275946	0.15802	3.959	3.841
$\langle 110 \rangle$ d	7318.342569	7276.601601	-0.275557	0.15747	3.960	3.842

Table 2: The total energy E_{def} of a simulation box containing a defect, the total energy E_{perf} of a perfect lattice simulation cell, the applied strain energy E^{app} , the elastic correction energy E_{el}^{corr} , and the formation energy E_{def}^F of a vacancy, a $\langle 100 \rangle$ dumbbell, an octahedral site interstitial, a $\langle 110 \rangle$ crowdion, and a $\langle 110 \rangle$ dumbbell in FCC gold. The value of E_{def}^F with no elastic correction, corresponding to $E^{app} = 0$ and $E_{el}^{corr} = 0$, is also given for comparison. All the values are given in eV units.

	P_{11}	P_{22}	P_{33}	P_{12}	P_{23}	P_{31}
Vac	-6.760	-6.760	-6.760	0.000	0.000	0.000
$\langle 100 \rangle$ d	36.667	39.612	39.612	0.000	0.000	0.000
Octa	39.371	39.984	39.984	0.000	0.000	0.000
$\langle 110 \rangle$ c	38.856	38.856	41.084	11.199	0.000	0.000
$\langle 110 \rangle$ d	38.742	38.742	41.332	11.155	0.000	0.000

Table 3: Elastic dipole tensor P_{ij} , in eV units, computed for a vacancy, a $\langle 100 \rangle$ dumbbell, an octahedral site interstitial, an $\langle 110 \rangle$ crowdion, and a $\langle 110 \rangle$ dumbbell in FCC gold.

	Ω_{11}	Ω_{22}	Ω_{33}	Ω_{12}	Ω_{23}	Ω_{31}	Ω_{rel}
Vac	-0.117	-0.117	-0.117	0.000	0.000	0.000	-0.351
$\langle 100 \rangle$ d	0.231	0.888	0.888	0.000	0.000	0.000	2.008
Octa	0.598	0.735	0.735	0.000	0.000	0.000	2.068
$\langle 110 \rangle$ c	0.520	0.520	1.018	1.062	0.000	0.000	2.058
$\langle 110 \rangle$ d	0.494	0.494	1.072	1.057	0.000	0.000	2.059

Table 4: Relaxation volume tensor Ω_{ij} and relaxation volume Ω_{rel} , in atomic volume units, computed for a vacancy, a $\langle 100 \rangle$ dumbbell, an octahedral site interstitial, a $\langle 110 \rangle$ crowdion, and a $\langle 110 \rangle$ dumbbell in FCC gold.

417 modification of the $5d$ bands [30, 31, 32]. The plane wave energy cut-off is
 418 450 eV for the 11 valence electrons included in the calculation. Different
 419 sizes of simulation cells were used for different defects. The corresponding
 420 box sizes and k-point meshes are given in Table 1. All the simulation boxes
 421 were relaxed to the stress-free condition, with residual forces lower than 0.01
 422 eV/Å. Formation energies were calculated using Eq. 18 with respect to a
 423 perfect crystal, using a similar cell size and the same k-point mesh.

424 Elastic constants are also required for calculating E^{app} and E_{el}^{corr} . They
 425 were calculated using the Le Page and Saxe method [33], using a 4-atom
 426 cubic cell. From *ab initio* calculations we obtained $C_{11} = 210.55\text{GPa}$, $C_{12} =$
 427 168.11GPa and $C_{44} = 49.96\text{GPa}$. These values are compatible with the
 428 low temperature experimental values, which are $C_{11} = 201.63\text{GPa}$, $C_{12} =$
 429 169.67GPa and $C_{44} = 45.44\text{GPa}$ [34]. The calculated lattice constant is
 430 4.075Å , whereas the experimental value is 4.07833Å [35].

431 The corrected defect formation energies E_{def}^F , applied strain energies E^{app} ,
 432 elastic correction energies E_{el}^{corr} , and the formation energy of defects with no
 433 correction applied, that is ignoring E^{app} and E_{el}^{corr} , are given in Table 2.
 434 It shows that a $\langle 100 \rangle$ dumbbell has the lowest formation energy, whereas a
 435 $\langle 110 \rangle$ crowdion has the lowest formation energy if the elastic correction is
 436 not included. However, we should note that the energy difference between a
 437 $\langle 100 \rangle$ dumbbell, a $\langle 110 \rangle$ crowdion and a $\langle 110 \rangle$ dumbbell is very small. Since
 438 the accuracy of a DFT calculation is in the meV range, it is hard to draw
 439 a definitive conclusion about the structure of the most stable SIA defect
 440 configuration in gold.

441 Elements of elastic dipole tensors P_{ij} , in eV units, are given in Table
 442 3, whereas the elements of the relaxation volume tensor Ω_{ij} and the total
 443 relaxation volume Ω_{rel} , in atomic volume units, are given in Table 4. We
 444 note that their values are correlated with the symmetry of a particular defect.
 445 Indeed, the calculated values of P_{ij} and Ω_{ij} might be more significant than the
 446 calculated values of the elastic correction terms. One can readily use them
 447 to evaluate the strength of defect-defect interactions through linear elasticity
 448 theory [5, 6, 7, 8, 9], and even apply it to examine the stress profile of an
 449 irradiated component on a macroscopic scale, if the distribution of defects is
 450 defined [17].

451 Elastic correction can also be applied to non-equilibrium configurations.
 452 For example, it can be applied to the atomic configurations describing the
 453 migration pathway of a defect. We performed a nudged elastic band calcula-
 454 tion [36, 37] of vacancy migration in gold, where seven NEB images were

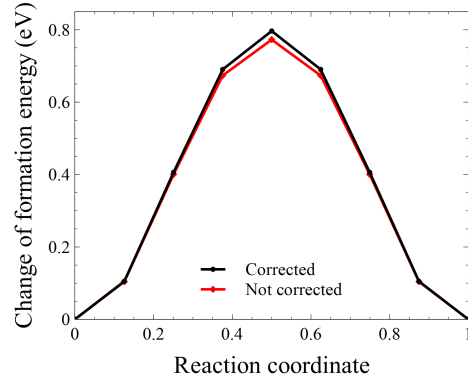


Figure 1: Variation of the formation energy of a vacancy during its transition from an equilibrium position to a nearest neighbour equilibrium position. A small difference can be observed between the cases studied with and without applying the elastic correction.

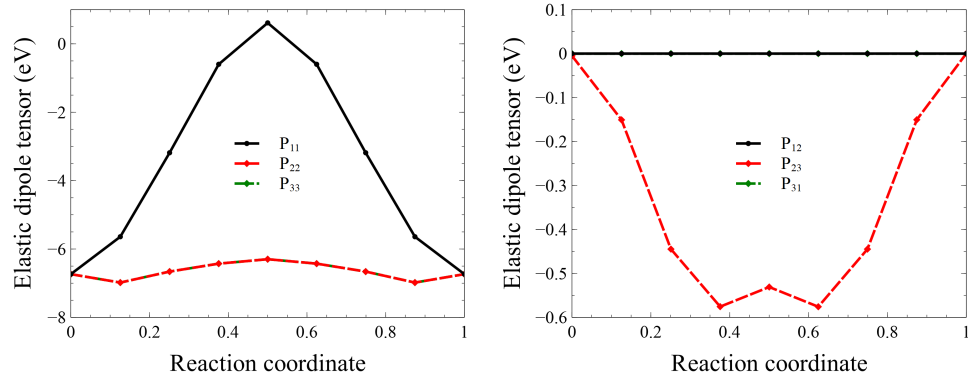


Figure 2: Elastic dipole tensor of a vacancy moving along a migration pathway in the $y-z$ plane. Owing to the symmetry of the defect, $P_{22} = P_{33}$ and $P_{12} = P_{31} = 0$.

455 used. A vacancy hops from an equilibrium position to the nearest neighbour
 456 equilibrium position in the $y-z$ plane. Fig. 1 shows the change in the forma-
 457 tion energy with and without the elastic energy correction. The computed
 458 migration energy agrees well with experimental value of $0.71 \pm 0.05\text{eV}$ [35].
 459 The effect of applying the elastic correction is not prominent in this case, as
 460 the stress field induced in the lattice by a vacancy is relatively weak.

461 On the order hand, we observe a change in P_{ij} during the transition, illus-
 462 trated in Fig. 2, which can give rise to effects of anisotropic diffusion under
 463 external stress, or the stress induced by other defects [38]. The anisotropic
 464 diffusion tensor in linear approximation of a spatially slow varying external
 465 strain field $\epsilon_{ij}(\mathbf{R})$ can be written, following Dederichs and Schroeder [39], as

$$D_{ij}(\mathbf{R}) = \frac{1}{2} \sum_h \lambda_h r_i^h r_j^h \exp\left(\frac{\epsilon_{kl}(\mathbf{R})(P_{kl}^{sd,h} - P_{kl}^{eq})}{k_B T}\right), \quad (32)$$

466 where h refers to a possible hopping site, $\lambda_h = \nu_0 \exp(-E_D^{M,h}/k_B T)$ is the
 467 atomic jump frequency, ν_0 is the attempt frequency, $E_D^{M,h}$ is the migration
 468 barrier, r_i^h is a Cartesian component of the hopping direction vector, $P_{kl}^{sd,h}$
 469 and P_{kl}^{eq} are the elastic dipole tensors at the saddle point and at an equilib-
 470 rium position. The value of D_{ij} for a given value of strain can be evaluated
 471 using the data given here. Anisotropic diffusion of point defects under ap-
 472 plied stress induced by a screw dislocation has been explored by Sivak and
 473 Sivak [40] in fcc copper using kinetic Monte Carlo simulations.

474 6.2. Molecular statics: Dislocation loop in tungsten

475 Elastic field of a mesoscopic defect is much stronger than that of a point
 476 defect. Elastic correction is also larger for a defect of larger size in a small
 477 simulation box. For example, an *ab initio* calculation is usually limited to a
 478 few hundred atoms. The formalism developed in this paper can be applied to
 479 any localized defect irrespective to its structure. If the elastic dipole tensor
 480 P_{ij} of the defect is known, one can use it to compute the corrected defect
 481 formation energy E_{def}^F using Eq. 18, provided that the strain field at the
 482 surface of a simulation box is approximated by linear elasticity. We would
 483 like to examine the convergence of the P_{ij} and E_{def}^F of mesoscopic scale defects
 484 as a function of simulation cell size and simulation conditions.

485 We have investigated the points using molecular statics. Molecular static
 486 allows us to do highly accurate calculations using very large simulation cells

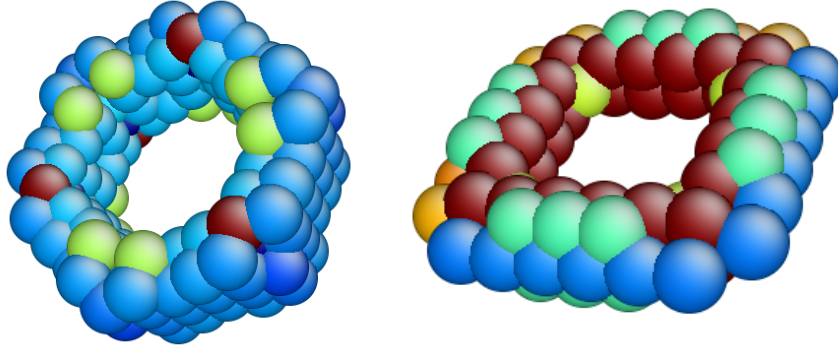


Figure 3: Atomic configuration of (left) a circular $\frac{1}{2}\langle 111 \rangle$ and (right) a square $\langle 100 \rangle$ self-interstitial atom loop. Both loops contain 61 self-interstitial atoms. Bulk atoms were filtered out according to the centre of symmetry parameter criterion.

487 within reasonable computation time. We used the Mason-Nguyen-Manh-
 488 Becquart (MNB) [41] potential for tungsten. The calculated elastic constants for this potential are $C_{11} = 526.83\text{GPa}$, $C_{12} = 205.28\text{GPa}$, and
 489 $C_{44} = 160.63\text{GPa}$. All the calculations were performed using LAMMPS [42].
 490 Atomic relaxations were performed using the conjugate gradient method. We
 491 have investigated circular $\frac{1}{2}\langle 111 \rangle$ self-interstitial atom (SIA) loops containing
 492 7, 13, 19, 37, 55 and 61 atoms, and square $\langle 100 \rangle$ SIA loops with 5, 13, 25,
 493 41 and 61 atoms, using simulation cells of varying size containing from 2,000
 494 to 1 million atoms. Two sets of calculations were performed. In one set,
 495 the shape and volume of the simulation cell remained fixed and the same as
 496 in the perfect lattice case. In the other set, the cell was permitted relax to
 497 a stress-free condition. The loop structure of a circular $\frac{1}{2}\langle 111 \rangle$ and square
 498 $\langle 100 \rangle$ loop with 61 atoms are shown in Fig. 3. They were generated using
 499 AtomEye [43], where bulk atoms were filtered using the centre of symmetry
 500 parameter criterion.
 501

502 Fig. 4 shows elements of the elastic dipole tensor of $\frac{1}{2}\langle 111 \rangle$ SIA loops
 503 plotted as functions of the simulation cell size. Due to the symmetry of the
 504 defect, values of diagonal terms are all the same and labelled $P_{\alpha\alpha}$, whereas
 505 the off-diagonal terms also have the same values and are labelled $P_{\alpha\beta}$. We
 506 see that both the fixed cell and stress-free condition calculations converge to
 507 the same value if the simulation box is large enough. Under the stress-free
 508 condition, when the simulation cell size is in the range of $10 \times 10 \times 10$ and
 509 $11 \times 11 \times 11$ unit cells, the cells containing 55 and 61 atoms loops deform

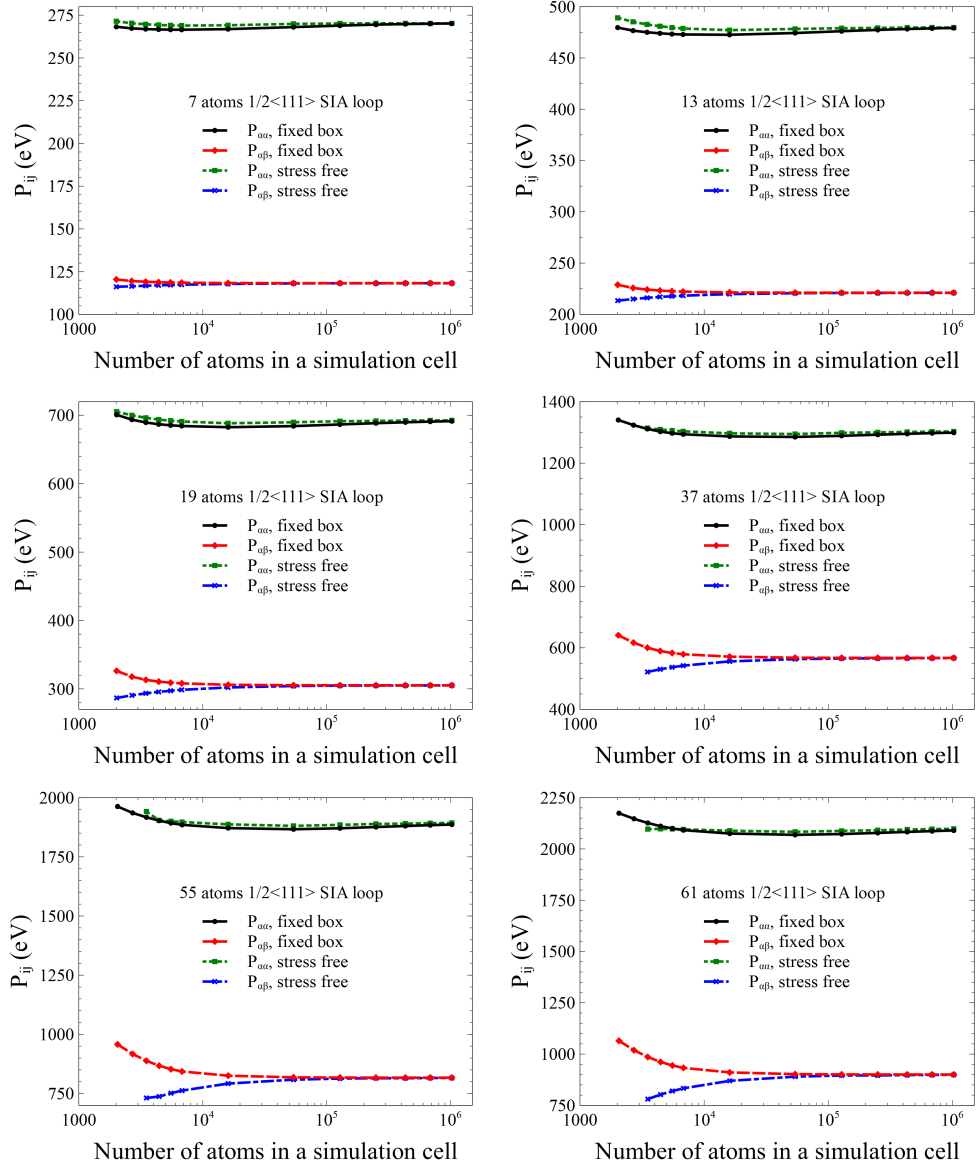


Figure 4: Elastic dipole tensors of $\frac{1}{2}\langle 111 \rangle$ self-interstitial atom loops containing 7, 13, 19, 37, 55, and 61 atoms as functions of the simulation cell size. $P_{\alpha\alpha}$ are the diagonal terms, whereas $P_{\alpha\beta}$ are the off-diagonal terms. Elements of the elastic dipole tensor are computed using the condition that the simulation cell shape was fixed to match the perfect lattice case, or allowed to relax to a stress-free condition.

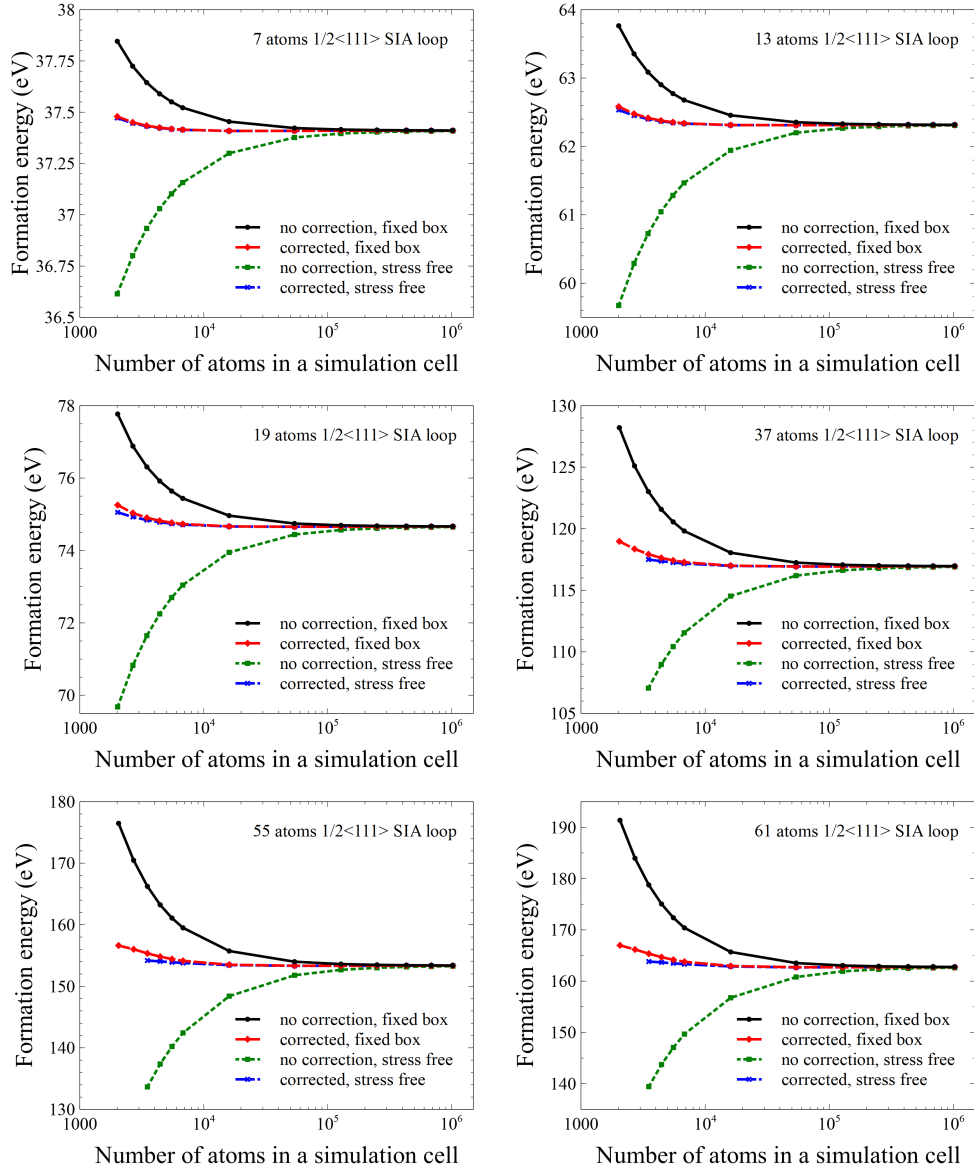


Figure 5: Formation energy E_{def}^F of $\frac{1}{2}\langle 111 \rangle$ self-interstitial atom loops containing 7, 13, 19, 37, 55, and 61 atoms shown as a function of the simulation cell size. The E_{def}^F is calculated with elastic correction applied, i.e. using Eq. 18, or without the correction, i.e. ignoring the E^{app} and E_{el}^{corr} . Both are calculated under the condition that the simulation cell shape was fixed to match the perfect lattice case, or was allowed to relax to a stress-free condition.

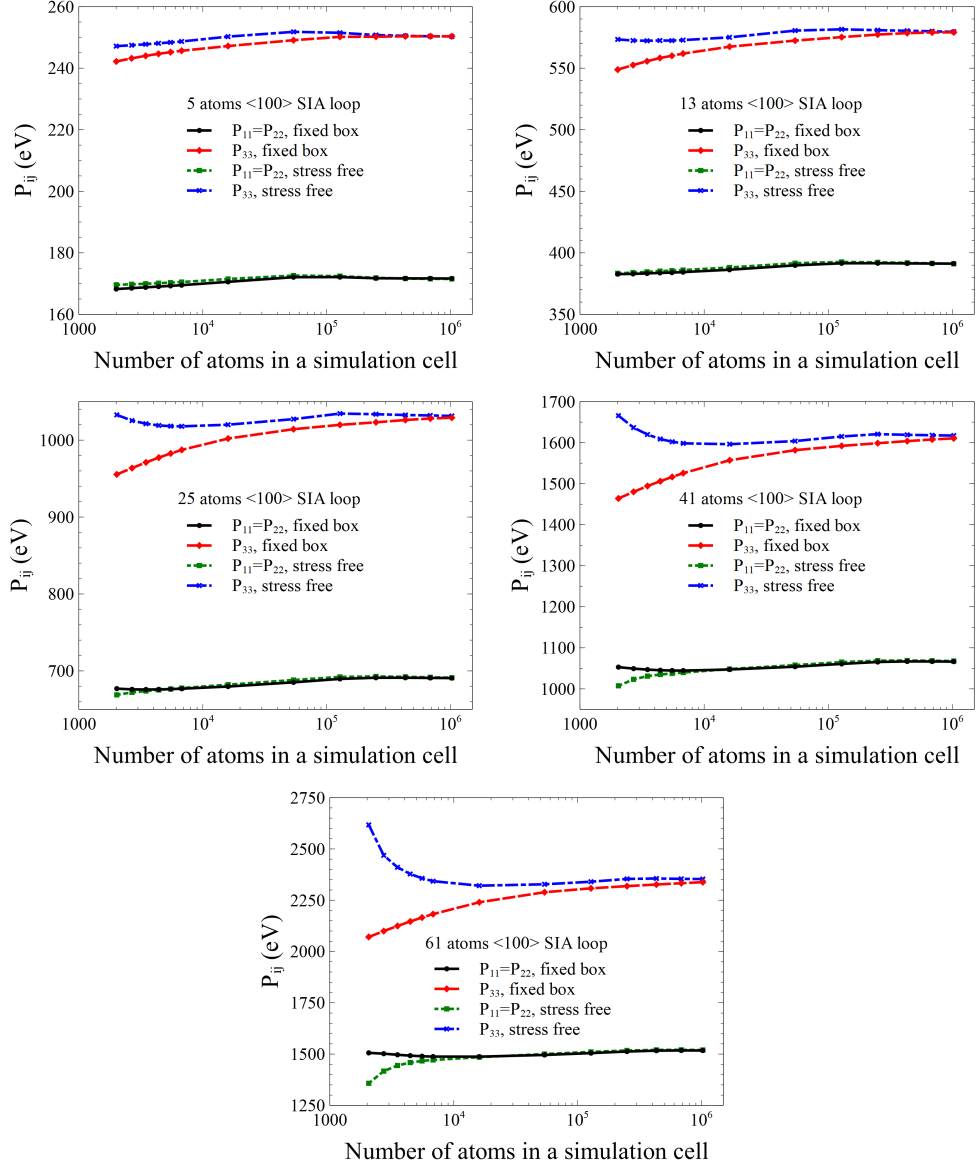


Figure 6: Elements of elastic dipole tensors of $\langle 100 \rangle$ self-interstitial atom loops containing 5, 13, 25, 41, and 61 atoms plotted as a function of the simulation cell size. The off-diagonal terms of the dipole tensor vanish because of symmetry. The elastic dipole tensor is calculated under the condition that the simulation box shape was fixed to match the perfect lattice case, or was allowed to relax to a stress-free condition.

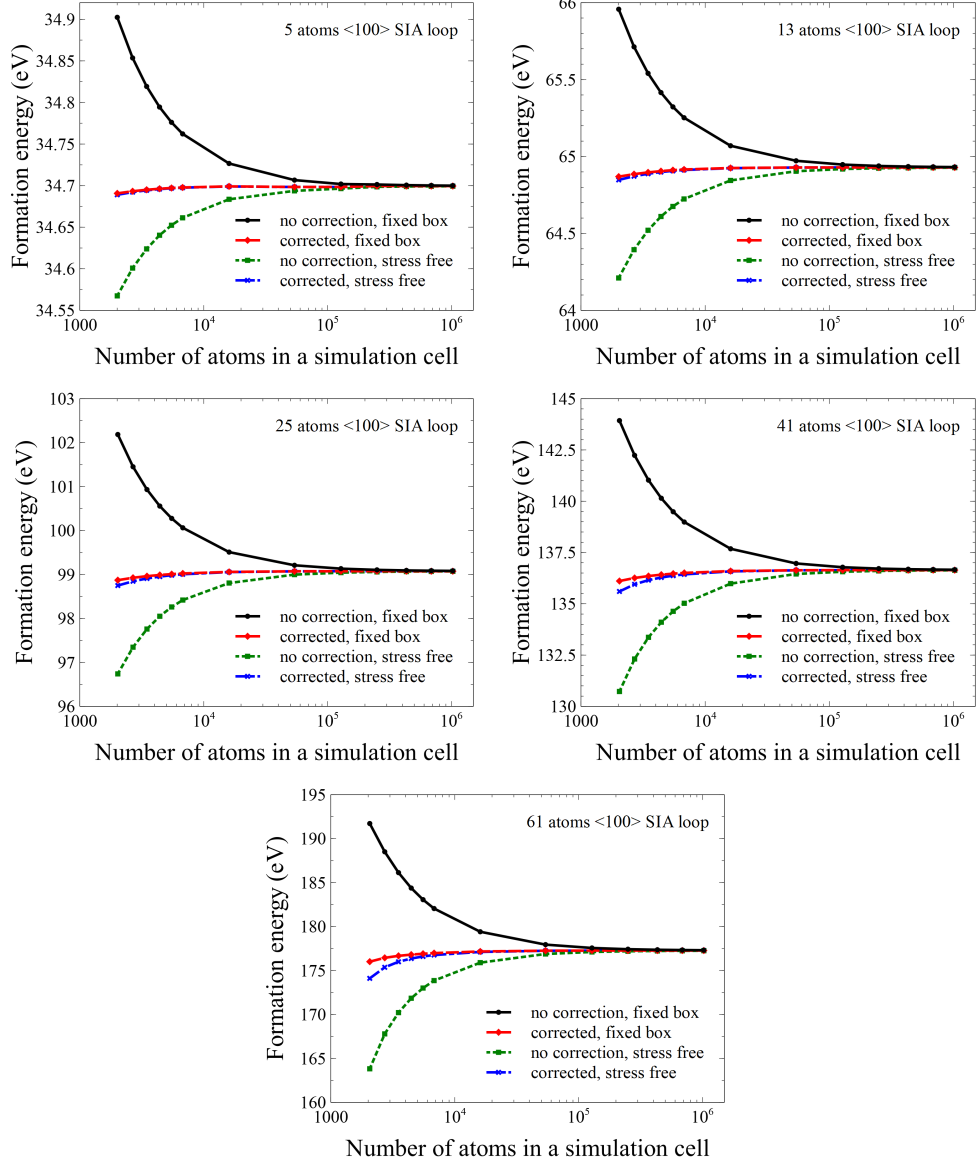


Figure 7: Formation energy E_{def}^F of $\langle 100 \rangle$ self-interstitial atom loops containing 5, 13, 25, 41, and 61 atoms shown as a function of the simulation cell size. Values of E_{def}^F were calculated with elastic correction applied, i.e. using Eq. 18, or with no correction, i.e. ignoring E^{app} and E_{el}^{corr} . Both were calculated under the condition that the simulation box shape was fixed to match the perfect lattice case, or was allowed to relax to a stress-free condition.

510 significantly. The calculated values of P_{ij} do not reflect the correct symmetry
511 of a $\frac{1}{2}\langle 111 \rangle$ SIA loop type, so we discarded these data.

512 Fig. 5 shows the corrected formation energy calculated using the data
513 shown in Fig. 4. We note that the elastic correction converges well in the
514 limit of large simulation box. At the same time, we see that although the
515 fixed cell and stress-free condition calculations suggest different values prior
516 to the application of elastic correction, their values become comparable when
517 this correction is applied. For mesoscopic scale loops, e.g. a 61 atom loop,
518 the difference can be fairly large if the correction is not applied.

519 Fig. 6 and 7 show elements of the dipole tensor and formation energy
520 of $\langle 100 \rangle$ loops as functions of the cell size. Due to symmetry, we know that
521 the elements of dipole tensor $P_{11} = P_{22}$, $P_{33} \neq 0$, and that the off-diagonal
522 elements all vanish. We observe a similar behaviour for $\langle 100 \rangle$ loops as for
523 $\frac{1}{2}\langle 111 \rangle$ loops. The error in P_{ij} becomes larger when the size of the defect
524 becomes comparable to the size of the simulation box. This is a consequence
525 of the fact that the derivation of the dipole tensor formalism is based on the
526 linear elasticity approximation.

527 When the size of the simulation cell is small, the deformation of the lattice
528 near the surface of the cell due to a defect may become large and hence non-
529 linear. This makes the values of P_{ij} computed in the linear elasticity theory
530 approximation inaccurate. Nevertheless, it still help correct the formation
531 energy for various simulation cell conditions, such as in the two limiting
532 cases of the fixed box and stress-free conditions. This enables calculating
533 the formation energy of a relatively large size defect using a relatively small
534 simulation cell with confidence, which is important especially in the context
535 of an *ab initio* calculation where the cost of computation is high.

536 7. Conclusion

537 In this study, we presented the fundamental theory, algorithms and nu-
538 merical implementation of computer program CALANIE, intended for the
539 evaluation of anisotropic elastic interaction energy under periodic boundary
540 conditions (PBCs). The theory is based on the linear elasticity approxi-
541 mation. The elastic interaction of a defect with its periodic images can be
542 approximated and evaluated using the elastic dipole and elastic Green's func-
543 tion formalism. The elements of elastic dipole tensor can be computed in the
544 same electronic or atomic scale simulation as the formation energy of the de-
545 fect. Elastic Green's function and its first and second derivatives can also be

546 calculated numerically if the values of elastic constants are known. Examples
547 with input files are given. Compilation of CALANIE can be performed using
548 any modern C++ compiler.

549 Applications of the program are illustrated using two case studies as ex-
550 amples. One example involves *ab initio* calculations of point defects in FCC
551 gold. We show that elastic correction can be applied not only to the equilib-
552 rium, but also to non-equilibrium configurations. Other applications involve
553 relatively large, mesoscopic scale defects. We investigate the convergence of
554 calculations of elements of dipole tensors and formation energies in the large
555 simulation cell limit. We show that the elastic correction treatment can im-
556 prove the quality of evaluation of the formation energy even in the limit
557 where the size of the defect is comparable with the size of the simulation cell.

558 **Acknowledgement**

559 This work has been carried out within the framework of the EUROfusion
560 Consortium and has received funding from the Euratom research and training
561 programme 2014-2018 and 2019-2020 under grant agreement No. 633053 and
562 from the RCUK Energy Programme [grant No. EP/I501045]. To obtain
563 further information on the data and models underlying the paper please
564 contact PublicationsManager@ccfe.ac.uk. The views and opinions expressed
565 herein do not necessarily reflect those of the European Commission.

- 566 [1] W. Cai, W. D. Nix, Imperfections in Crystalline Solids, Cambridge Uni-
567 versity Press, Cambridge, England, UK, 2016.
- 568 [2] A. E. Sand, K. Nordlund, S. L. Dudarev, Radiation damage produc-
569 tion in massive cascades initiated by fusion neutrons in tungsten, Jour-
570 nal of Nuclear Materials 455 (1) (2014) 207–211, proceedings of the
571 16th International Conference on Fusion Reactor Materials (ICFRM-
572 16). doi:<https://doi.org/10.1016/j.jnucmat.2014.06.007>.
- 573 [3] A. E. Sand, M. J. Aliaga, M. J. Caturla, K. Nordlund, Surface effects
574 and statistical laws of defects in primary radiation damage: Tungsten
575 vs. iron, Europhysics Letters 115 (3) (2016) 36001. doi:[10.1209/0295-
576 5075/115/36001](https://doi.org/10.1209/0295-5075/115/36001).
- 577 [4] J. Byggmästar, F. Granberg, A. E. Sand, A. Pirttikoski, R. Alexander,
578 M.-C. Marinica, K. Nordlund, Collision cascades overlapping with self-

- 579 interstitial defect clusters in Fe and W, *Journal of Physics: Condensed*
580 *Matter* 31 (24) (2019) 245402. doi:10.1088/1361-648X/ab0682.
- 581 [5] S. L. Dudarev, M. R. Gilbert, K. Arakawa, H. Mori, Z. Yao, M. L.
582 Jenkins, P. M. Derlet, Langevin model for real-time brownian dynamics
583 of interacting nanodefects in irradiated metals, *Phys. Rev. B* 81 (2010)
584 224107. doi:10.1103/PhysRevB.81.224107.
585 URL <https://link.aps.org/doi/10.1103/PhysRevB.81.224107>
- 586 [6] C. Varvenne, F. Bruneval, M.-C. Marinica, E. Clouet, Point defect mod-
587 eling in materials: Coupling ab initio and elasticity approaches, *Phys.*
588 *Rev. B* 88 (2013) 134102. doi:10.1103/PhysRevB.88.134102.
- 589 [7] C. Varvenne, E. Clouet, Elastic dipoles of point defects
590 from atomistic simulations, *Phys. Rev. B* 96 (2017) 224103.
591 doi:10.1103/PhysRevB.96.224103.
- 592 [8] S. L. Dudarev, P.-W. Ma, Elastic fields, dipole tensors, and interaction
593 between self-interstitial atom defects in bcc transition metals, *Phys. Rev.*
594 *Materials* 2 (2018) 033602. doi:10.1103/PhysRevMaterials.2.033602.
- 595 [9] P.-W. Ma, S. L. Dudarev, Universality of point defect structure in
596 body-centered cubic metals, *Phys. Rev. Materials* 3 (2019) 013605.
597 doi:10.1103/PhysRevMaterials.3.013605.
598 URL <https://link.aps.org/doi/10.1103/PhysRevMaterials.3.013605>
- 599 [10] M. Durrand-Charre, *Microstructure of Steels and Cast Irons*, Springer-
600 Verlag, Berlin, 2003.
- 601 [11] W. Kohn, L. J. Sham, Self-consistent equations including ex-
602 change and correlation effects, *Phys. Rev.* 140 (1965) A1133–A1138.
603 doi:10.1103/PhysRev.140.A1133.
604 URL <https://link.aps.org/doi/10.1103/PhysRev.140.A1133>
- 605 [12] P. Hohenberg, W. Kohn, Inhomogeneous electron gas, *Phys. Rev.* 136
606 (1964) B864–B871. doi:10.1103/PhysRev.136.B864.
607 URL <https://link.aps.org/doi/10.1103/PhysRev.136.B864>
- 608 [13] D. R. Mason, X. Yi, M. A. Kirk, S. L. Dudarev, Elastic trapping of
609 dislocation loops in cascades in ion-irradiated tungsten foils, *Journal of*

- 610 Physics: Condensed Matter 26 (37) (2014) 375701. doi:10.1088/0953-
611 8984/26/37/375701.
- 612 [14] G. Subramanian, D. Perez, B. P. Uberuaga, C. N. Tomé, A. F. Voter,
613 Method to account for arbitrary strains in kinetic monte carlo simula-
614 tions, Phys. Rev. B 87 (2013) 144107. doi:10.1103/PhysRevB.87.144107.
615 URL <https://link.aps.org/doi/10.1103/PhysRevB.87.144107>
- 616 [15] E. Martínez, M. J. Caturla, J. Marian, Dft-parameterized object kinetic
617 monte carlo simulations of radiation damage, in: W. Andreoni, S. Yip
618 (Eds.), Handbook of Materials Modeling: Applications: Current and
619 Emerging Materials, Springer International Publishing, Cham, 2018, pp.
620 1–32. doi:10.1007/978-3-319-50257-1_137-1.
- 621 [16] G. Leibfried, N. Breuer, Point Defects in Metals, Springer, Berlin, 1978.
- 622 [17] S. L. Dudarev, D. R. Mason, E. Tarleton, P.-W. Ma, A. E. Sand, A multi-
623 scale model for stresses, strains and swelling of reactor components under
624 irradiation, Nuclear Fusion 58 (12) (2018) 126002. doi:10.1088/1741-
625 4326/aadb48.
- 626 [18] C. Domain, C. S. Becquart, Ab initio calculations of defects in
627 Fe and dilute Fe–Cu alloys, Phys. Rev. B 65 (2001) 024103.
628 doi:10.1103/PhysRevB.65.024103.
- 629 [19] E. Clouet, S. Garruchet, H. Nguyen, M. Perez, C. S. Becquart,
630 Dislocation interaction with C in α -Fe: A comparison between atomic
631 simulations and elasticity theory, Acta Materialia 56 (14) (2008) 3450
632 – 3460. doi:<https://doi.org/10.1016/j.actamat.2008.03.024>.
633 URL <http://www.sciencedirect.com/science/article/pii/S1359645408002218>
- 634 [20] T. Jourdan, Simulation of macroscopic systems with non-vanishing elas-
635 tic dipole components, Journal of the Mechanics and Physics of Solids
636 125 (2019) 762 – 773. doi:<https://doi.org/10.1016/j.jmps.2019.02.002>.
637 URL <http://www.sciencedirect.com/science/article/pii/S0022509618309827>
- 638 [21] D. M. Barnett, The precise evaluation of derivatives of the anisotropic
639 elastic Green’s functions, physica status solidi (b) 49 (2) 741–748.
640 doi:10.1002/pssb.2220490238.

- 641 [22] W. Cai, V. V. Bulatov, J. Chang, J. Li, S. Yip, Periodic image effects
642 in dislocation modelling, *Philosophical Magazine* 83 (5) (2003) 539–567.
643 doi:10.1080/0141861021000051109.
- 644 [23] G. Kresse, J. Hafner, Ab initio molecular dynamics for liquid metals,
645 *Phys. Rev. B* 47 (1993) 558–561. doi:10.1103/PhysRevB.47.558.
646 URL <https://link.aps.org/doi/10.1103/PhysRevB.47.558>
- 647 [24] G. Kresse, J. Hafner, Ab initio molecular-dynamics simulation of the
648 liquid-metal–amorphous-semiconductor transition in germanium, *Phys.*
649 *Rev. B* 49 (1994) 14251–14269. doi:10.1103/PhysRevB.49.14251.
650 URL <https://link.aps.org/doi/10.1103/PhysRevB.49.14251>
- 651 [25] G. Kresse, J. Furthmüller, Efficiency of ab initio total energy
652 calculations for metals and semiconductors using a plane-wave ba-
653 sis set, *Computational Materials Science* 6 (1) (1996) 15 – 50.
654 doi:[https://doi.org/10.1016/0927-0256\(96\)00008-0](https://doi.org/10.1016/0927-0256(96)00008-0).
655 URL <http://www.sciencedirect.com/science/article/pii/0927025696000080>
- 656 [26] G. Kresse, J. Furthmüller, Efficient iterative schemes for ab initio total-
657 energy calculations using a plane-wave basis set, *Phys. Rev. B* 54 (1996)
658 11169–11186. doi:10.1103/PhysRevB.54.11169.
659 URL <https://link.aps.org/doi/10.1103/PhysRevB.54.11169>
- 660 [27] F. Hofmann, E. Tarleton, R. J. Harder, N. W. Phillips, P.-W. Ma, J. N.
661 Clark, I. K. Robinson, B. Abbey, W. Liu, C. E. Beck, 3d lattice dis-
662 tortions and defect structures in ion-implanted nano-crystals, *Scientific*
663 *Reports* 7 (2017) 45993. doi:10.1038/srep45993.
- 664 [28] J. P. Perdew, A. Ruzsinszky, G. I. Csonka, L. A. Constantin,
665 J. Sun, Workhorse semilocal density functional for condensed matter
666 physics and quantum chemistry, *Phys. Rev. Lett.* 103 (2009) 026403.
667 doi:10.1103/PhysRevLett.103.026403.
668 URL <https://link.aps.org/doi/10.1103/PhysRevLett.103.026403>
- 669 [29] J. Sun, M. Marsman, G. I. Csonka, A. Ruzsinszky, P. Hao, Y.-S. Kim,
670 G. Kresse, J. P. Perdew, Self-consistent meta-generalized gradient ap-
671 proximation within the projector-augmented-wave method, *Phys. Rev.*
672 *B* 84 (2011) 035117. doi:10.1103/PhysRevB.84.035117.
673 URL <https://link.aps.org/doi/10.1103/PhysRevB.84.035117>

- 674 [30] A. D. Corso, A. M. Conte, Spin-orbit coupling with ultrasoft pseudopo-
675 tentials: Application to au and pt, Phys. Rev. B 71 (2005) 115106.
676 doi:10.1103/PhysRevB.71.115106.
677 URL <https://link.aps.org/doi/10.1103/PhysRevB.71.115106>
- 678 [31] N. E. Christensen, B. O. Seraphin, Relativistic band calculation and
679 the optical properties of gold, Phys. Rev. B 4 (1971) 3321–3344.
680 doi:10.1103/PhysRevB.4.3321.
681 URL <https://link.aps.org/doi/10.1103/PhysRevB.4.3321>
- 682 [32] T. Rangel, D. Kecik, P. E. Trevisanutto, G.-M. Rignanese,
683 H. Van Swygenhoven, V. Olevano, Band structure of gold from
684 many-body perturbation theory, Phys. Rev. B 86 (2012) 125125.
685 doi:10.1103/PhysRevB.86.125125.
686 URL <https://link.aps.org/doi/10.1103/PhysRevB.86.125125>
- 687 [33] Y. Le Page, P. Saxe, Symmetry–general least–squares extraction of elas-
688 tic data for strained materials from ab initio calculations of stress, Phys.
689 Rev. B 65 (2002) 104104. doi:10.1103/PhysRevB.65.104104.
690 URL <https://link.aps.org/doi/10.1103/PhysRevB.65.104104>
- 691 [34] J. R. Neighbours, G. A. Alers, Elastic constants of silver and gold, Phys.
692 Rev. 111 (1958) 707–712. doi:10.1103/PhysRev.111.707.
693 URL <https://link.aps.org/doi/10.1103/PhysRev.111.707>
- 694 [35] P. Ehrhart, P. Jung, H. Schultz, H. Ullmaier, Landolt-Börnstein -
695 Group III Condensed Matter · Volume 25: “Atomic Defects in Metals”,
696 Springer-Verlag Berlin Heidelberg, 1991. doi:10.1007/10011948_45.
- 697 [36] G. Mills, H. Jansson, G. K. Schenter, Reversible work transition state
698 theory: application to dissociative adsorption of hydrogen, Surface
699 Science 324 (2) (1995) 305 – 337. doi:[https://doi.org/10.1016/0039-](https://doi.org/10.1016/0039-6028(94)00731-4)
700 [6028\(94\)00731-4](https://doi.org/10.1016/0039-6028(94)00731-4).
701 URL <http://www.sciencedirect.com/science/article/pii/0039602894007314>
- 702 [37] H. Jónsson, G. Mills, K. W. Jacobsen, Nudged elastic band method for
703 finding minimum energy paths of transitions, World Scientific, 1998,
704 pp. 385–404. doi:10.1142/9789812839664_0016.
705 URL https://www.worldscientific.com/doi/abs/10.1142/9789812839664_0016

- 706 [38] P.-W. Ma, S. L. Dudarev, Effect of stress on vacancy formation and
707 migration in body-centred-cubic metals, *Physical Review Materials*.
- 708 [39] P. H. Dederichs, K. Schroeder, Anisotropic diffusion in stress fields,
709 *Phys. Rev. B* 17 (1978) 2524–2536. doi:10.1103/PhysRevB.17.2524.
710 URL <https://link.aps.org/doi/10.1103/PhysRevB.17.2524>
- 711 [40] A. B. Sivak, P. A. Sivak, Efficiency of dislocations as sinks of radiation
712 defects in fcc copper crystal, *Crystallography Reports* 59 (3) (2014) 407–
713 414. doi:10.1134/S1063774514030183.
714 URL <https://doi.org/10.1134/S1063774514030183>
- 715 [41] D. R. Mason, D. Nguyen-Manh, C. S. Becquart, An empirical potential
716 for simulating vacancy clusters in tungsten, *Journal of Physics: Con-*
717 *densed Matter* 29 (50) (2017) 505501. doi:10.1088/1361-648x/aa9776.
- 718 [42] S. Plimpton, Fast parallel algorithms for short-range molecular dy-
719 namics, *Journal of Computational Physics* 117 (1) (1995) 1 – 19.
720 doi:<https://doi.org/10.1006/jcph.1995.1039>.
721 URL <http://www.sciencedirect.com/science/article/pii/S002199918571039X>
- 722 [43] J. Li, AtomEye: an efficient atomistic configuration viewer, *Modelling*
723 *and Simulation in Materials Science and Engineering* 11 (2) (2003) 173–
724 177. doi:10.1088/0965-0393/11/2/305.